

Pt/Ga-SBA-15 composites synthesis and characterization

R. Hernández Morales, J. G. Pacheco Sosa*, J. G. Torres Torres,
H. Pérez Vidal, M. A. Lunagómez Rocha, D. De la Cruz Romero
División Académica de Ciencias Básicas, Universidad Juárez Autónoma de Tabasco (UJAT)
Cunduacán, Tabasco, 86690, México.

J. Escobar Aguilar#
Instituto Mexicano del Petróleo
G. A. Madero, Cd. de México, 07730, México

M.C. Barrera
Facultad de Ciencias Químicas-Centro de Investigación en Recursos Energéticos y Sustentables, Universidad Veracruzana
Coatzacoalcos, Veracruz, 96538, México
(Received: September 23rd, 2019; Accepted: March 16th, 2020)

Pt (0.5, 1 and 1.5 wt%) was impregnated by incipient wetness on SBA-15 and corresponding Ga-modified (3, 5, 10 and 20 wt%) composites. Gallium nitrate was incorporated directly during the mesoporous siliceous network synthesis. Materials were characterized by N₂ physisorption, X-ray diffraction, Fourier transformed infrared spectroscopy, scanning electron microscopy and transmission electron microscopy. SBA-15 had surface area greater than 800 m²/g that decreased by Ga incorporation in binary materials. It seemed that tetrahedral gallium was well-incorporated into mesoporous silica walls. Pt dispersion slightly diminished (as to that on SBA-15) by augmenting Ga concentration in composites. Corresponding pore size maxima shifted to lower diameters (as to that of non-impregnated supports) after platinum loading suggesting Pt crystals inside pores of SBA-15 and Ga-modified carriers. Large cubic platinum crystals were observed over all prepared materials probably due to sintering (during calcining at 500 °C) of metallic particles weakly interacting with the carriers surface. After materials annealing (500 °C under static air) metallic platinum was evidenced (by XRD) pointing out to noble metal reduction that could be facilitated by decomposition of organic remains from Si alkoxide used during supports synthesis which presence was ascertained by FTIR.

Introduction

Siliceous mesoporous materials have received much attention due to their multiple potential applications in adsorption phenomena and catalysis. The mesoporous molecular sieve SBA-15 (Santa Barbara Amorphous) exhibits interesting characteristics as high surface area (600-1000 m²/g), thick walls (3-6 nm) and significant hydrothermal stability [1]. Also, Pluronic P123 structure-directing surfactant (non-ionic poly(ethylene glycol)-block-poly(propylene glycol)-blockpoly(ethylene glycol), average molecular mass ~ 5800 Da [2]), used during its synthesis is cheap, biodegradable and non-toxic [3]. Silica precursors like tetra-alkoxysilane, fumed silica and water glass could be used during SBA-15 synthesis but some of those SiO₂ sources are either expensive or toxic [4]. Thus, low cost eco-friendly silica precursors are essential to curtail costs of SBA-15 manufacturing at large scale. For instance, using sugar leaf ash as low cost raw material for SBA-15 synthesis has been reported [5]. Also, cheap sodium metasilicate has been utilized to that end [6]. For sake of simplicity, however, tetraethyl orthosilicate (TEOS) is probably the most used silica source during lab-scale fundamental investigations on those ordered matrices. That type of siliceous structured solid has been studied as catalysts support due to its uniform mesoporous network that could facilitate interaction of deposited active phases with bulky molecules to be transformed. However, as that of any other SiO₂-based

matrix SBA-15 surface itself is not particularly adequate to disperse deposited active phases mainly due to its inertness [7], and very low acidity. Indeed, that pure siliceous solid consists of an electronically neutral framework that lacks Brønsted acidity [8]. Thus, a considerable number of efforts has been focused on functionalizing that rather inert siliceous surface. Some previous reports have found that Ga-addition to SBA-15 materials could render solids of weak Lewis acidity [9], which amount increased with gallium content in binary formulations, although Brønsted sites creation has also been identified by Ga incorporation into mesoporous networks [10]. Absence of strong acid sites could be reflected in enhanced stability (in the liquid-phase acylation of benzoyl chloride with anisole, for instance [9]), as carbonaceous deposits deposition could be relieved, as to those formed over more acidic surfaces (those of zeolites, for example). However, acidity (type, number and strength) of prepared composites clearly depend upon method of gallium component introduction [11], which offered possibility of obtaining binary solids of tailor-made surface properties. One important variable during preparation of SBA-15-based materials modified by inorganic additives is the synthesis pH. For instance, gallium precursors remain in cationic form under acidic conditions used during SBA-15 synthesis (commonly below pH 1). Under those circumstances Ga introduction into the mesostructured solid walls seems to be difficult to achieve. Also, at low pH Ga³⁺ cations could neither polymerize nor condense [12]. Also, under strongly

*jose.pacheco@ujat.mx, #jeaguila@imp.mx

acidic environment, gallium could hardly be incorporated into SBA-15 framework due to unfavored condensation reaction between gallium hydrate cations and cationic silicate oligomer. As low pH (~1) is required to promote silica precursors condensation there could be a compromise between obtaining high-quality hexagonally ordered SBA-15 and proper gallium incorporation into the mesostructured matrix. For the former enough hydrogen bonding is needed whereas electrostatic interaction between the surfactant and the galliosilicate oligomer could be favored at higher pH [13]. Thus, defining optimal conditions for Ga-modified SBA-15 preparation remains an ongoing challenge.

Regarding gallium-modified siliceous mesoporous matrices used as catalysts support of metallic phases Ni/Ga (1-3 wt%)-MCM41 has been prepared and tested in methane dry reforming [14], finding that Ga incorporation was reflected in decreased number of both strong and medium basic sites. Also, carbon deposition under reaction conditions diminished with gallium addition. However and in spite of their interesting properties, to the best of our knowledge, the effect of Ga addition at various concentrations on the properties of SBA-15 binary solids intended to be used as metallic Pt support has not been addressed in the open literature. In this work, Ga-modified SBA-15 matrices at various gallium loadings (3, 5, 10 and 20 wt%) were prepared by directly adding corresponding nitrate during TEOS-based SBA-15 synthesis. Pt was deposited (0.5, 1 and 1.5 wt%) by pore-filling impregnation on obtained composites to assess the effect of Ga addition on platinum dispersion. Materials were characterized through several physicochemical instrumental techniques to elucidate their textural, structural and surface properties.

Experimental

Material synthesis

Ga-modified SBA-15

SBA-15 mesoporous materials were synthesized following a well-known preparation protocol [1]. Thus, triblock copolymer Pluronic P123 (OE₂₀OP₇₀OE₂₀ non-ionic surfactant, Sigma-Aldrich, 98 wt%, 19.2 g) was diluted in 450 ml of water and 300 ml of HNO₃ (0.5 M, Meyer, 70 wt%) solution were further added. The transparent mixture was kept under vigorous stirring for 24 h at 35 °C. Tetraethyl orthosilicate (TEOS, Sigma-Aldrich, 98 wt%, 40 ml) was used as Si source. After TEOS addition the obtained sol was kept under stirring (600 rpm, ~62 rad/s) for 24 h. Then, the sol was submitted to hydrothermal treatment at 80 °C for 72 h. The obtained gel was filtered, washed with distilled water and dried at room temperature. In order to prepare Ga-modified samples Ga(NO₃)₃·H₂O (Sigma-Aldrich, 99.9 wt%) was simultaneously added with TEOS. The amount of gallium salt utilized corresponded to various Ga contents (3, 5, 10 and 20 wt%) in binary solids. All solids were finally calcined at 500 °C for 6 h (2 °C/min heating rate) to obtain mixed oxide composites. Various prepared materials were identified by Ga(x)-SBA-15 key where x stands for Ga wt% in composites.

Pt impregnation

Pt (0.5, 1.0 and 1.5 wt%) was deposited over SBA-15 and corresponding Ga-modified composites by pore-filling impregnation using chloroplatinic acid (H₂PtCl₆ hydrate, Aldrich, 99.9 wt%) as precursor salt. Impregnated solids were left aging for 24 h at room temperature to allow Pt ions diffusion through composites porous network. Materials were further annealed at 500 °C (6 h, 2 °C/min heating rate). After annealing under mentioned conditions residual Cl⁻ from Pt salt could be totally eliminated. Indeed, Miura *et al.* [15], found essentially not chloride residue (as determined by X-ray fluorescence) after calcination at 500 °C of Pt/SiO₂ samples obtained from H₂PtCl₆ impregnation. Various prepared materials were identified by Pt(y)/Ga(x)-SBA-15 key where y stands for impregnated Pt wt% on composites.

Materials characterization

Textural properties of various prepared materials were determined by N₂ physisorption (-198 °C) by using a Micromeritics Tristar II 3020 equipment. Studied solids were previously degassed during 4 h (300 °C) to eliminate adsorbed species. Surface area and pore size distribution (PSD) of various studied solids were determined by BET (Brunauer-Emmett-Teller) and BJH (Barret-Joyner-Halenda, desorption data branch) methods, respectively. Structural order of samples was studied by powder X-ray diffraction utilizing a Bruker D8-Advance diffractometer (CuK α radiation, $\lambda = 1.5418 \text{ \AA}$) at 35 kV accelerating voltage, 25 mA and 0.020° steps. Samples were analyzed by Fourier transformed infrared spectroscopy (FTIR) with a Shimadzu IRAffinity-1 apparatus in the 340-4000 cm⁻¹ range at 2 cm⁻¹ resolution and 40 scans. Acquired data were processed by using IRsolutionTM software. Wafers were prepared by mixing samples (at 5 wt%) to be studied with KBr (Sigma Aldrich, FTIR grade). Particles morphology was observed by scanning electron microscopy (SEM) in JEOL JSM-6010LA apparatus at 20 kV accelerating voltage, high vacuum and at various magnifications. Obtained micrographs were processed by using InTouchScope™ software. Materials were characterized by high-resolution transmission electron microscopy (HR-TEM) carried out in JEOL 2100 field emission electron microscope operating at 200 kV with LaB₆ filament (spherical aberration coefficient, Cs = 0.5 mm). Micrographs were taken in bright field mode. Prior to analysis powdered samples were ultrasonically dispersed in isopropyl alcohol and then some drops of obtained suspension were supported on lacey carbon coated copper grids (3.05 mm of diameter).

Results and discussion

Textural properties

SBA-15 and corresponding Ga-modified solids (excepting the material with the lowest Ga content) had type IV N₂ adsorption isotherms (Figure 1a) with H1 hysteresis as defined by the International Union of Pure and Applied Chemistry (IUPAC) [16] those isotherm profiles being typical of mesostructured matrices containing cylindrical pores of uniform section [17]. Hystereses loop shape of

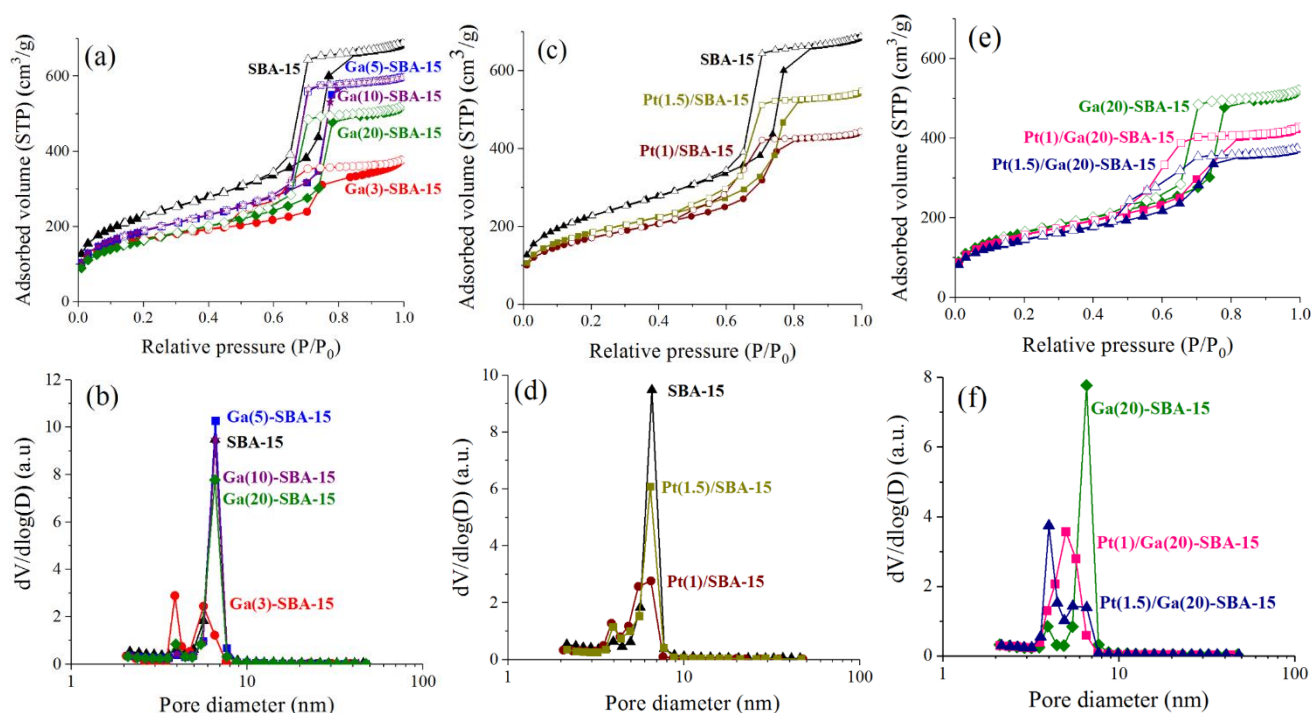


Figure 1. N₂ adsorption isotherms (at -198 °C) and pore size distribution (BJH profiles), corresponding to (a) and (b) pristine SBA-15 and Ga-modified supports at various gallium contents; (c) and (d) Pt(1.0 and 1.5 wt%)/SBA-15; (e) and (f) SBA-15 modified with 20 wt% Ga and corresponding Pt impregnated (1.0 and 1.5 wt%) solids.

Ga(3)-SBA-15 was intermediate between H1 and H2-type probably by influence of some Ga₂O₃ segregated domains. Textural characteristics of various prepared solids (mixed supports and corresponding Pt-impregnated materials) are shown in Tables 1 and 2. Pristine mesoporous SBA-15 had typical texture with 819 m²/g surface area (S_{BET}), pore volume (V_p) of 1.05 cm³/g and average pore diameter (from corresponding PSD, Figure 1b) of 5.55 nm. Those properties nicely corresponded to expected values for SBA-15 matrices (500 < S_{BET} < 1300 m²/g, 0.82 < V_p < 1.69 cm³/g) commonly reported in the literature for such type of mesostructured SiO₂ [18].

However, all Ga-modified solids at various contents had decreased surface area as to that of pristine SBA-15. Fifth column of Table 1 shows theoretical surface area of composites considering incorporation of essentially non-porous Ga₂O₃ component in SBA-15 matrix (^bS_{BET}), pointing out to that in samples of the lowest Ga content gallium oxide domains could be partially plugging well-ordered mesoporous siliceous network.

Table 1. Textural properties of SBA-15 and various Ga-SBA-15 materials prepared.

Sample	S _{BET} (m ² /g)	V _p (cm ³ /g)	^a D _p (nm)	^b S _{BET} (m ² /g)	S _{BET} / ^b S _{BET}
SBA-15	819	1.05	5.55	-	-
Ga(3)-SBA-15	590	0.57	3.89, 5.5	786	0.75
Ga(5)-SBA-15	676	0.92	5.80	764	0.88
Ga(10)-SBA-15	681	0.89	5.79	709	0.96
Ga(20)-SBA-15	586	0.79	5.42	599	0.98

^a From BJH plot, desorption branch data.

^b Theoretical value considering well-dispersed non-porous Ga₂O₃ phase component.

Conversely, samples with Ga at 10 and 20 wt% had S_{BET} completely similar to corresponding ^bS_{BET} ones strongly suggesting absence of clogged pores due to well-dispersed Ga phases integrated to mesoporous siliceous matrix. Unaffected shape of adsorption isotherms in those cases supported that assumption (Figure 1a). In this line, gallium inclusion (in tetrahedral coordination) into siliceous SBA-15 well-ordered mesoporous structure has been identified (by ⁷¹Ga NMR spectroscopy) by others [19] when studying modified SBA-15 materials at various Ga contents and prepared through different synthesis methodologies. Launay *et al.* [19], also reported better incorporation of gallium at higher content in SBA-matrices where in samples at Si/Ga of

Table 2. Textural properties of Pt supported on SBA-15 and various Ga-SBA-15 materials prepared.

Sample	S _{BET} (m ² /g)	V _p (cm ³ /g)	^a D _p (nm)	^b S _{BET} (m ² /g)	S _{BET} / ^b S _{BET}
Pt(0.5)/SBA-15	684	0.86	3.89, 5.60	815	0.84
Pt(1)/SBA-15	609	0.68	3.89, 4.80	811	0.75
Pt(1.5)/SBA-15	642	0.84	3.89, 5.40	807	0.80
Pt(1.5)/Ga(3)-SBA-15	633	0.53	3.89, 4.00	581	1.00
Pt(1)/Ga(20)-SBA-15	562	0.62	4.7	580	0.97
Pt(1.5)/Ga(20)-SBA-15	518	0.54	3.9, 5.2	577	0.90

^a From BJH plot, desorption branch data.

^b Theoretical value considering well-dispersed non-porous Pt deposition.

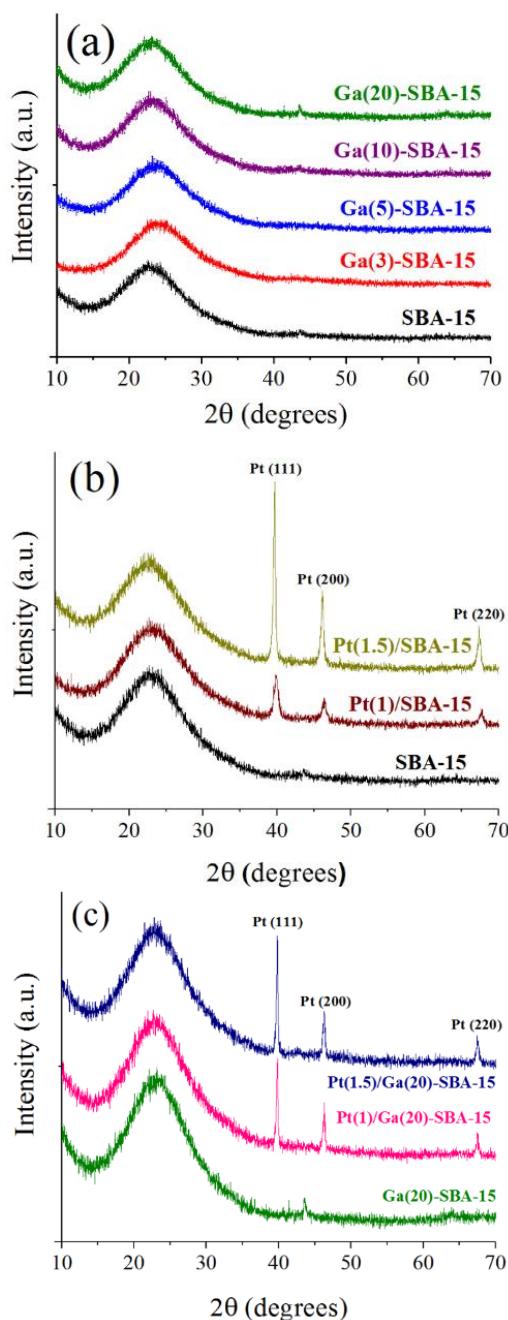


Figure 2. Wide-angle X-ray diffraction patterns of SBA-15, Ga-modified SBA-15 at various gallium contents and corresponding Pt-impregnated solids. (a) SBA-15 and Ga-modified binary supports; (b) Pt-impregnated on pristine SBA-15; (c) Pt-impregnated on Ga(20)-SBA-15.

5 and 10 (very similar composition to our materials with 5 and 10 Ga wt%) the latter solid had higher Ga proportion incorporated in the mesoporous tetrahedral matrix. Probably at enhanced Ga^{3+} concentration there could be better adjustment of the hydrolysis rates of the Si and Ga starting materials [19].

With the sole exception of binary solid at the lowest gallium content PSD profiles of Ga-modified solids (Figure 1b) showed maxima at around 5.8 nm (Table 1) similar to that of parent SBA-15 pointing out to efficient integration of Ga^{3+} into walls of siliceous mesoporous network.

Nevertheless, the former binary solid also had additional maximum at lower diameter (~ 3.89 nm) suggesting deposition of gallium domains insides SBA-15 pores.

The lower closing partial pressure of hysteresis loop of corresponding N_2 physisorption isotherm as to that of pristine silica support (Figure 1a) was in full agreement with aforementioned finding. Following the same way of reasoning, alike shifts in hysteresis closing of Pt-impregnated SBA-15 (Figure 1c) strongly suggested presence of noble metal particles inside pristine siliceous porous matrix [20]. After Pt loading on SBA-15 surface area and pore volume importantly diminished ($\sim 20\%$, Table 2). As those losses were much higher than expected considering deposition of non-porous phases that could indicate low platinum dispersion that provoked partial pore plugging of siliceous networks. Accordingly, Kumar *et al.* [21] reported that Pt impregnation (1.3 wt%) by pore filling on SBA-15 could render supported solids of rather large particle size (~ 21 nm) provoking significantly decreased texture by occluded porosity. Corresponding pore size distributions profiles (Figure 1d) showed contributions from smaller pores as to those of non-impregnated siliceous carrier that could be rationalized by considering presence of some Pt crystals inside the carrier porous network.

The S_{BET} of sample of the highest Ga content was just slightly affected by Pt deposition (Figure 1e and Table 2) suggesting decreased plugging of carrier pores. Also, very defined shift of PSD to lower diameters (see hystereses loop closing in isotherms shifted to lower P/P_0 values and corresponding pore size profiles, (Figure 1f) strongly suggested Pt crystals inside pores of that Ga-modified SBA-15 composite.

X-ray diffraction

A wide signal identified in the $15\text{--}35^\circ$ 2θ range observed in diffractograms of all studied samples corresponded to amorphous silica constituting SBA-15 walls [22], Figure 2a. No reflexions related to Ga_2O_3 defined domains were identified on any binary support (Figure 2a) pointing out to absence of defined gallium oxide crystals. Although existence of well-dispersed oxidic gallium domains (undetectable by XRD) could not be ruled out that fact suggested good integration of Ga^{3+} species into the walls of mesoporous tetrahedral silicon oxide network [23]. Conversely, reflections due to Ga_2O_3 crystals has been reported [23] in the case of samples where gallium was deposited at 10 wt% (through corresponding nitrate as salt precursor) by post-synthesis impregnation on SBA-15 matrix.

Pt impregnated solids showed three main reflections at 2θ values of 39.8 , 46.1 and 67.8° assigned to interplanar distances of (111), (200) and (220) face-centered cubic metallic platinum facets (PDF 01-087-0640), Figures 2b and 2c. Unexpectedly, no supported PtOx species were found. In the opposite, metallic Pt^0 was evidenced.

Finding reduced platinum in calcined samples (see subsection *Pt impregnation*) supported on SBA-15 has been reported (as determined by XPS analysis) in the past by others [24], although no explanation was advanced in that

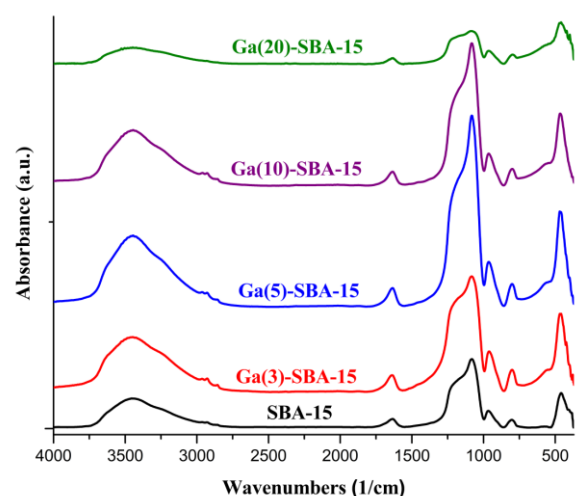
Table 3. Crystal size (as determined by Scherrer formula using Pt(111) reflection) of various Pt-impregnated materials prepared.

Sample	Crystallite size (nm)
Pt(0.5)/SBA-15	7.78
Pt(1)/SBA-15	8.58
Pt(1.5)/SBA-15	18.85
Pt(1)/Ga(3)-SBA-15	16.39
Pt(1.5)/Ga(3)-SBA-15	23.33
Pt(1)/Ga(5)-SBA-15	20.64
Pt(1.5)/Ga(5)-SBA-15	24.04
Pt(1)/Ga(10)-SBA-15	18.77
Pt(1.5)/Ga(10)-SBA-15	26.69
Pt(1)/Ga(20)-SBA-15	21.77
Pt(1.5)/Ga(20)-SBA-15	23.93

case. Organic remains that could be present in our mixed materials could play a determining role on that fact. Indeed, organic residua from Si alkoxides used during SBA-15 and corresponding Ga-modified solids synthesis usually could remain occluded in calcined materials [25]. Those organic species could contribute to Pt reduction during high-temperature annealing. Indeed, organic compounds had been successfully applied by others as noble metals reductants [26].

According to Scherrer formula and by using the most intense Pt (111) reflection corresponding crystal size for solids with SBA-15 and Ga-modified ones as carrier were estimated, Table 3. Platinum crystal size on pristine siliceous support increased from 7.78 to 18.85 nm with Pt loading from 0.5 to 1.5 wt%. Others have reported [20] similar values to the last one when studying samples with 4 wt% platinum attributing that to low interaction of deposited species with silanol groups on silica surface. Due to that, in addition to low Pt dispersion after impregnation significant metallic particles sintering during high-temperature annealing could take place. Also, low noble metal dispersion could justify significant S_{BET} loss of SBA-15-supported samples, much larger to those expected considering noble metal loading (see column 6 of Table 2). In these cases, Pt crystals dimensions were clearly big enough to plug some pores ($D_p \sim 5.8$ nm, Table 1) of the pristine siliceous carrier.

Ga addition in SBA-15 matrix was detrimental on Pt dispersion as to that on SBA-15 carrier, Table 3. For materials at 1 wt% Pt loading crystal size increased from 8.58 (on pristine siliceous support) to 21.77 nm in the solid of the highest Ga content. Although that could be ascribed to much lower S_{BET} of binary supports as to that of pristine SBA-15 (for instance, 586 versus 819 m^2/g for material with 20 wt% Ga and pristine mesoporous solid, respectively, Table 1) it was clear that gallium modification did not favorably altered surface properties of mixed oxides obtained. In the opposite to that found, incorporation of gallium in tetrahedral network in SBA-15 matrix resulted in improved vanadium species dispersion, being that attributed to better anchorage of those species on a more acidic support (as compared to pristine silica-based one) [23]. It is worth noting that Ga incorporation method used in mentioned investigation (gallium impregnation at various loadings on a pre-formed siliceous matrix) probably could play a decisive

**Figure 3.** FTIR spectra of pristine SBA-15 and Ga-modified supports at various gallium contents.

role on noble metal dispersion. Further work is needed on this point to elucidate the reason behind observed behavior. Finally, it seemed that due to the presence of organic remains (that could contribute to impregnated platinum reduction during annealing conditions under air) the reduction step under H_2 flow (at 300-400 °C) [27,28] could be avoided simplifying then the catalyst activation procedure.

FTIR spectroscopy

Broad bands centered around 3453 and 1633 cm^{-1} were attributed to stretching vibrations of surface hydroxyl groups and water [29] and to deformation vibration of adsorbed undissociated H_2O molecules coordinated to surface centers [30], Figure 3. Shoulder at 3685 cm^{-1} in all spectra could be related to surface silanol groups [31]. Absorptions at 2970 and 2857 cm^{-1} related to $-CH_3$ degenerated stretching mode and $-CH_2$ stretching symmetrical vibrations, respectively, indicated organic remains from Si alkoxides used during support synthesis [25]. As mentioned in previous section, those organic remains could contribute in reducing deposited platinum species supported on the prepared composites. Peak at around 10814 cm^{-1} corresponded to Si-O-Si asymmetric stretching vibration meanwhile bands at ~ 803 and 458 cm^{-1} were originated by symmetric stretching and deformation modes of aforementioned bonds. Band at 967 cm^{-1} was related to Si-OH stretching vibrations [29]. No infrared absorptions corresponding to Ga_2O_3 defined domains could be established (Figure 3), in agreement with that found by XRD (Figure 2a). Band at 458 cm^{-1} in studied spectra could be related to Si-O-Si bending vibrations [32].

Scanning electron microscopy

SBA-15 morphology exhibited particles of around 3-4 μm in diameter formed by numerous agglomerated hexagonal platelets of 800-1000 nm (not shown), completely similar to that previously reported [33]. Smooth platelets of very short length in axial direction were evidenced. In full agreement, others [34] identified alike morphology for SBA-15 prepared under similar conditions as to those used in the present

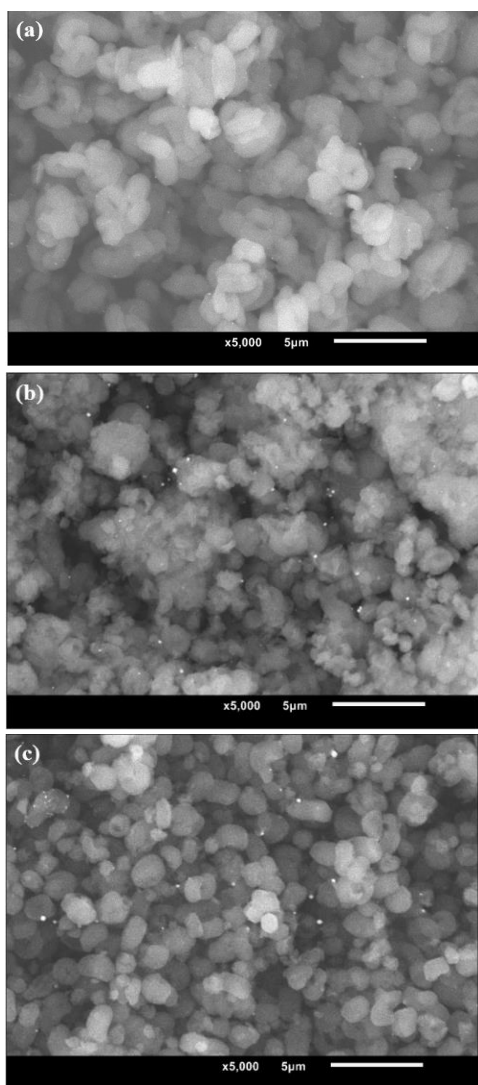


Figure 4. SEM micrographs, 5000 \times , scale bar: 5 μm . (a) Pt(1.5)/SBA-15; (b) Pt(1.5)/Ga(3)-SBA-15; (c) Pt(1.5)/Ga(20)-SBA-15.

investigation. No significant differences on morphology as to that of pristine SBA-15 was observed after Pt impregnation, Figure 4a.

However, Ga-modified materials seemed to be constituted by smaller agglomerates of otherwise similar shape as to those observed in the SBA-15 case, Figures 4b and 4c. It was apparent that a good gallium proportion could be well-integrated in tetrahedral silica matrix. In this line, to efficiently incorporate aluminum into siliceous framework the heteroatoms must be available as highly reactive species during multidentate binding stage of mesoporous SiO_2 synthesis. Regarding Al-modified MCM-41 solids, it has been claimed that [35] highly charged aluminum species could be coordinated with surfactant molecules, other cationic species or aqueous silicate oligomers being then readily introduced into the silica framework. In full agreement to that it has been found [36] that aluminum was better integrated into MCM-41 frameworks when $\text{Al}_2(\text{SO}_4)_3$ was used as salt precursor (as opposed to $\text{AlO}(\text{OH})$). It could be then that Ga^{3+} cations (from corresponding nitrate utilized, see sub-section *Ga-modified SBA-15*) were well-

incorporated to SBA-15 due to similar aforementioned synthesis mechanism.

Interestingly, morphology of particles constituting the Ga material of the highest heteroatom content (Figure 4c) showed certain resemblance to that of mesoporous gallium oxide phases prepared from gallium nitrate hydrate with non-ionic tri-blockcopolymer F127 as structure directing agent [37]. Indeed, it has been proposed [38] that the self-assembly process could be controlled by the electrostatic charge matching between the inorganic ions in solution (Ga^{3+}), non-ionic surfactants and inorganic counterions (NO_3^-). Gallium hydroxo species could be assembled then through hydrogen bonding with hydronium ion solvated neutral block copolymers (as Pluronic P123). Thus, under synthesis conditions used in this work formation of mesoporous gallium oxide domains could not be ruled out. Deeper studies on this topic are obviously required.

Bright spots due to platinum crystals were clearly registered in micrographs of Ga-modified materials (Figures 4b and 4c) attesting noble metal particles of low dispersion.

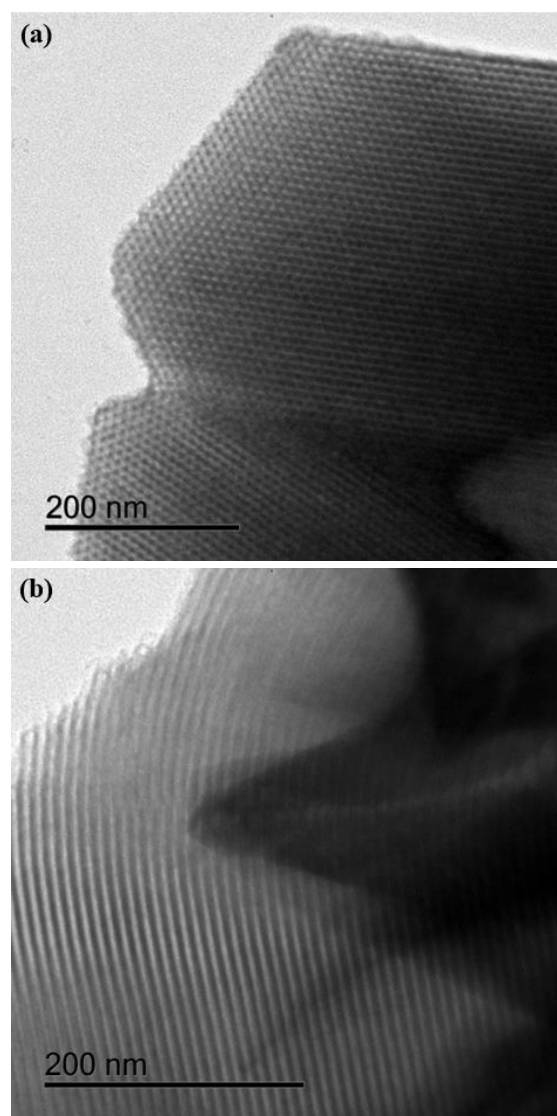


Figure 5. HR-TEM micrographs. (a) as prepared SBA-15, along pore axis direction; (b) Ga(20)-SBA-15, perpendicular to pore axis direction.

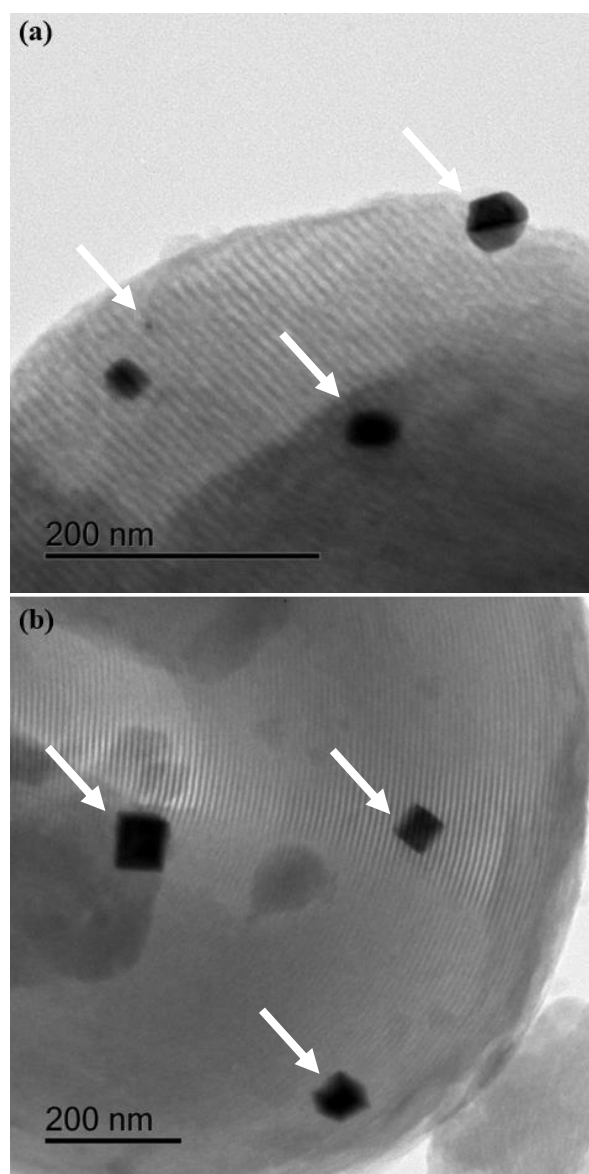


Figure 6. HR-TEM micrographs of platinum-impregnated materials. (a) Pt(1.5)/SBA-15; (b) Pt(1.5)/Ga(20)-SBA-15. Arrows: Platinum crystals.

High-resolution TEM

The highly ordered honeycomb-shaped mesoporous structure of siliceous pristine SBA-15 containing hexagonal cross sections with pores of around 6 nm (Table 1) was evidenced in Figure 5a. That characteristic 2-D hexagonal symmetry ($p6mm$) was in full agreement with corresponding structural characterization of SBA-15 materials as presented in previous works [32, 39]. Although our materials were not characterized by low-angle XRD we considered that shape of corresponding N_2 adsorption isotherms (Figure 1a) and studies by high resolution HR-TEM (Figure 5) clearly evidenced the mesoporous ordered structure corresponding to SBA-15-type materials. That array was well- preserved in the composite of the highest Ga content (Figure 5b) in full agreement with the unaltered shape of corresponding N_2 physisorption isotherm, Figure 1a, as to that of pristine SiO_2 matrix pointing out to good incorporation of tetrahedral Ga^{3+} in silica framework. No defined segregated Ga_2O_3 domains

were identified in accordance with our XRD findings (Figure 2a).

Large cubic platinum crystals were found on SBA-15 (Figure 6a). Those particles could result from sintering (particle migration-coalescence [40]) under annealing at 500 °C (see sub-section *Pt impregnation*) of noble metal particles originally deposited on the external siliceous carrier surface. They could be prone to sintering due to their weak interaction with the ordered SiO_2 surface.

Presence of those crystals large enough to partially plug some pores of binary supports could explain surface area lost of Pt(1.5)/SBA-15 much bigger than expected considering noble metal loading (20% diminished S_{BET} , as to that of corresponding to $^bS_{BET}$, Table 2). Some small platinum crystal inside mesoporous network were also observed in the Pt(1.5)/SBA-15 sample, Figure 6b. Larger noble metal particles were observed for Pt(1.5)/Ga(20)-SBA-15, Figure 6b, supporting that found through crystal size calculations (Table 3) were enhanced noble metal crystallites size as to those on pristine SBA-15 of similar loading was estimated. Thus, no positive effect of Ga addition to SBA-15 matrices on platinum dispersion was corroborated. Although surface acidity could be incorporated to SBA-15 by gallium addition those sites could be of rather mild acid properties [9] not being strong enough to interact with supported noble metal particles. Indeed, hydrocracking reactions that require strong acidity were avoided on sulfided NiW/Ga-SBA-15 tested in dibenzothiophene hydrodesulfurization [41] evidencing absence of those sites.

In our case, platinum crystals sintering at the annealing conditions used in the present work could not be precluded presumably due to their weak interaction with those weak acid surface sites. Interestingly some amorphous inclusions could be observed in Figure 6b pointing out to some segregated gallium oxide domains. However, they were not detectable by XRD (Figure 2a) due to their amorphousness.

Conclusions

Pt (0.5, 1 and 1.5 wt%) was impregnated by incipient wetness on SBA-15 and corresponding Ga-modified (3, 5, 10 and 20 wt%) composites. Gallium nitrate was used to incorporate Ga directly during the mesoporous siliceous network synthesis. SBA-15 had surface area greater than 800 m^2/g that decreased by Ga incorporation in binary materials. It seemed that in most samples (but in the one of the lowest gallium content) a good proportion of tetrahedral Ga was well-incorporated into mesoporous silica walls. Pt dispersion diminished (as to that on SBA-15) by augmenting Ga concentration in composites. Corresponding pore size maxima shifted to lower diameters (as to that of non-impregnated supports) after platinum loading suggesting Pt crystals inside pores of SBA-15 and Ga-modified carriers, that effect being more evident in the latter. Large cubic platinum crystals (25-50 nm) were observed over all prepared materials probably due to sintering (during calcining at 500 °C) of metallic particles weakly interacting with the carriers surface. After materials annealing (500 °C under static air) metallic platinum was evidenced (by XRD)

pointing out to noble metal reduction during decomposition of organic remains from Si alkoxide used during carriers synthesis which presence was ascertained by FTIR. No positive effect of Ga addition in SBA-15 matrices on platinum dispersion was observed.

Acknowledgements

R. Hernández Morales acknowledges UJAT-DACB and IMP for their support on carrying out the present investigation. He is also grateful to CONACYT (Mexico) by Master in Science scholarship provided (639499).

References

- [1]. K. Flodström, V. Alfredsson, *Micropor. Mesopor. Mat.* **59**, 167 (2003).
- [2]. E.M. Björk, *J. Chem. Educ.* **94**, 91 (2017).
- [3]. S. Singh, R. Kumar, R., H.D. Setiabudi, S. Nanda, *Appl. Catal. A-Gen.* **559**, 57 (2018).
- [4]. V. Meynen, P. Cool, E.F. Vansant, *Micropor. Mesopor. Mater.* **125**, 170 (2009).
- [5]. A. Arumugam, V. Ponnusami, *J. Sol-Gel Sci. Techn.* **67**, 244 (2013).
- [6]. J.J. Kim, G.D. Stucky, *Chem. Commun.* **13**, 1159 (2000).
- [7]. P.F. Wang, H.X. Jin, M. Chen, D.F. Jin, B. Hong, H.L. Ge, J. Gong, X.L. Peng, H. Yang, Z.Y. Liu, X.Q. Wang, *J. Nanomater.* **2012**, 269861 (2012).
- [8]. R. Huirache-Acuña, R. Nava, C.L. Peza-Ledesma, J. Lara-Romero, G. Alonso-Núñez, B. Pawelec, E.M. Rivera-Muñoz, *Materials* **6**, 4139 (2013).
- [9]. Z. El Berrichi, L. Cherif, O. Orsen, J. Fraissard, J.P. Tessonnier, E. Vanhaecke, B. Louis, M.J. Ledoux, C. Pham-Huu, *Appl. Catal. A-Gen.* **298**, 194 (2006).
- [10]. M.J. Gracia, E. Losada, R. Luque, J.M. Campelo, D. Luna, J.M. Marinas, A.A. Romero, *Appl. Catal. A-Gen.* **349**, 148 (2008).
- [11]. Z. El Berrichi, B. Louis, J.P. Tessonnier, O. Ersen, L. Cherif, M.J. Ledoux, C. Pham-Huu, *Appl. Catal. A-Gen.* **316**, 219 (2007).
- [12]. L. Rivoira, M.L. Martínez, O. Anunziata, A. Beltramone, *Micropor. Mesopor. Mat.* **254**, 96 (2017).
- [13]. C.-F. Cheng, C.-H. Cheng, *Stud. Surf. Sci. Catal.* **156**, 133 (2005).
- [14]. A.S. Al-Fatesh, A.A. Ibrahim, J.K. Abu-Dahrieh, A.S. Al-Awadi, A.M. El-Toni, A.H. Fakeeha, A.E. Abasaeed, *Catalysts* **8**, 229 (2018).
- [15]. S. Kaneko, M. Izuka, A. Takahashi, M. Ohshima, H. Kurokawa, H. Miura, *Appl. Catal. A-Gen.* **427-428**, 85 (2012).
- [16]. K.S.W. Sing, D.H. Everett, R.A.W. Haul, L. Moscou, R.A. Pierotti, J. Rouquérol, T. Siemieniewska, *Pure Appl. Chem.* **57**, 603 (1985).
- [17]. S.G. Leofanti, M. Padovan, G. Tozzola, B. Venturelli, *Catal. Today* **41**, 207 (1998).
- [18]. A.J. Schwanke, C. Favero, R. Balzer, K. Bernardo-Gusmão, S.B.C. Pergher, *J. Braz. Chem. Soc.* **29**, 328 (2018).
- [19]. F. Launay, B. Jarry, J.L. Bonardet, *Appl. Catal. A-Gen* **368**, 132 (2009).
- [20]. Y. Yin, Z.F. Yang, Z.H. Wen, A.H. Yuan, X.Q. Liu, Z.Z. Zhang, H. Zhou, *Sci. Rep.* **7**, 4509 (2017).
- [21]. M.S. Kumar, D. Chen, J.C. Walmsley, A. Holmen, *Catal. Commun.* **9**, 747 (2008).
- [22]. R. Palcheva, L. Kaluža, L. Dimitrov, G. Tyuliev, G. Avdeev, K. Jirátová, A. Spojakina, *Appl. Catal. A-Gen.* **520**, 24 (2016).
- [23]. L.P. Rivoira, J. Cussa, M.L. Martínez, A.R. Beltramone, *Catal. Today, in press, available* (2018).
- [24]. D. Ballesteros-Plata, A. Infantes-Molina, E. Rodríguez-Castellón, *Appl. Catal. A-Gen.* **580**, 93 (2019).
- [25]. J. Escobar, J.A. De los Reyes, T. Viveros, *Ind. Eng. Chem. Res.* **39**, 666 (2000).
- [26]. Y. Shiraiishi, H. Tanaka, H. Sakamoto, S. Ichikawa, T. Hirai, *RSC Adv.* **7**, 6187 (2017).
- [27]. M.Y. Kim, S.B. Jung, M.G. Kim, Y.S. You, J.-H. Park, C.-H. Shin, G. Seo, *Catal. Lett.* **129**, 194 (2009).
- [28]. B. Li, Z. Xu, W. Chu, S. Luo, F. Jing, *Chinese J. Catal.* **38**, 726 (2017).
- [29]. Z. Wang, F. Zhang, Y. Yang, B. Xue, J. Cui, N. Guan, *Chem. Mater.* **19**, 3286 (2007).
- [30]. C. Morterra, *J. Chem. Soc. Faraday Trans. 1* **84**, 1617 (1988).
- [31]. G.W. Griffith, *Ind. Eng. Chem. Prod. Res. Dev.* **23**, 590 (1984).
- [32]. F. Azimov, I. Markova, V. Stefanova, Kh. Sharipov, *J. Univ. Chem. Technol. Metallurgy* **47**, 333 (2012).
- [33]. G. Morales Hernández, J.G. Pacheco Sosa, J. Escobar Aguilar, J.G. Torres Torres, H. Pérez Vidal, M.A. Lunagómez Rocha, D. De la Cruz Romero, P. del Ángel Vicente, *Rev. Mex. Ing. Chem.* **19**, 997 (2019).
- [34]. Y. Qin, Y. Wang, H. Wang, J. Gao, Z. Qu, *Procedia Environ. Sci.* **18**, 366 (2013).
- [35]. M. Janicke, D. Kumar, G.D. Stucky, B.F. Chmelka, *Stud. Surf. Sci. Catal.* **84**, 243 (1994).
- [36]. A. Hernández, J. Escobar, J.G. Pacheco, J.A. de los Reyes, M.C. Barrera, *Rev. Soc. Quím. Méx.* **48**, 260 (2004).
- [37]. C.A. Deshmane, J.B. Jasinski, M.A. Carreon, *Eur. J. Inorg. Chem.* **2009**, 3275 (2009).
- [38]. C.A. Deshmane, J.B. Jasinski, M.A. Carreon, *Micropor. Mesopor. Mat.* **130**, 97 (2010).
- [39]. J. Zhu, T. Wang, X. Xu, *Appl. Catal. B- Environ.* **130-131**, 197 (2013).
- [40]. J. Liu, Q. Ji, T. Imai, K. Ariga, H. Abeb, *Sci. Rep.* **7**, 41773 (2017).
- [41]. A. Olivas, P.A. Luque, C.M. Gómez-Gutiérrez, D.L. Flores, R. Valdez, L. Escalante, P. Schach, R. Silva-Rodrigo, *Catal. Commun.* **91**, 67 (2017).

© 2020 by the authors; licensee SMCTSM, Mexico. This article is an open access article distributed under the terms and conditions of the Creative Commons Attribution license (<http://creativecommons.org/licenses/by/4.0/>).